HAL open science

High-resolution study of oscillator strengths and predissociation rates for 13C18O

Michèle Eidelsberg, Jean-Louis Lemaire, Steven R. Federman, Alan N. Heays, Glenn Stark, James R. Lyons, Lisseth Gavilan, Nelson de Oliveira

To cite this version:

Michèle Eidelsberg, Jean-Louis Lemaire, Steven R. Federman, Alan N. Heays, Glenn Stark, et al.. High-resolution study of oscillator strengths and predissociation rates for 13C18O. Astronomy and Astrophysics - A&A, 2017, 602, A76 (13 p.). 10.1051/0004-6361/201630195 . insu-01562620

HAL Id: insu-01562620

https://insu.hal.science/insu-01562620v1

Submitted on 11 Nov 2020

HAL is a multi-disciplinary open access archive for the deposit and dissemination of scientific research documents, whether they are published or not. The documents may come from teaching and research institutions in France or abroad, or from public or private research centers.

L'archive ouverte pluridisciplinaire **HAL**, est destinée au dépôt et à la diffusion de documents scientifiques de niveau recherche, publiés ou non, émanant des établissements d'enseignement et de recherche français ou étrangers, des laboratoires publics ou privés.

A&A 602, A76 (2017)
DOI: 10.1051/0004-6361/201630195
© ESO 2017

Astronomy & Astrophysics

High-resolution study of oscillator strengths and predissociation rates for $^{13}C^{18}O$

W-X bands and Rydberg complexes between 92.9 and 93.5 nm

M. Eidelsberg[1], J. L. Lemaire[2], S. R. Federman[3], A. N. Heays[1,4], G. Stark[5], J. R. Lyons[6], L. Gavilan[7], and N. de Oliveira[8]

[1] Observatoire de Paris, LERMA, UMR 8112 du CNRS, 75014 Meudon, France
e-mail: michele.eidelsberg@obspm.fr
[2] Institut des Sciences Moléculaires d'Orsay (ISMO), CNRS – Université Paris-Sud (UMR 8214), 91405 Orsay, France
e-mail: jean-louis.lemaire@u-psud.fr
[3] Department of Physics and Astronomy. University of Toledo, Toledo, OH 43606, USA
e-mail: steven.federman@utoledo.edu
[4] Leiden Observatory, Leiden University, 2300 RA Leiden, The Netherlands
[5] Department of Physics, Wellesley College, Wellesley, MA 02481, USA
[6] School of Earth and Space Exploration, Arizona State University, Tempe, AZ 85281, USA
[7] Université Versailles St-Quentin; Sorbonne Universités, UPMC Université Paris 06; CNRS/INSU, LATMOS-IPSL, 78280 Guyancourt, France
[8] DESIRS beamline, Synchrotron SOLEIL, 91192 Saint-Aubin, France

Received 5 December 2016 / Accepted 25 January 2017

ABSTRACT

We carried out experiments at the SOLEIL synchrotron facility to acquire data for modelling CO photochemistry in the vacuum ultraviolet. We report oscillator strengths and predissociation rates for four vibrational bands associated with transitions from the $v = 0$ level of the $X^1\Sigma^+$ ground state to the $v = 0$–3 vibrational levels of the core excited $W^1\Pi$ Rydberg state, and for three overlapping bands associated with the 4pπ, 5pπ, and 5pσ Rydberg states between 92.9 and 93.4 nm in $^{13}C^{18}O$. These results complete those obtained in the same conditions for $^{12}C^{16}O$, $^{13}C^{16}O$, and $^{12}C^{18}O$ recently published by us, and extend the development of a comprehensive database of line positions, oscillator strengths, and linewidths of photodissociating transitions for CO isotopologues. Absorption spectra were recorded using the Vacuum UltraViolet Fourier Transform Spectrometer (VUV-FTS) installed on the Dichroïsme Et Spectroscopie par Interaction avec le Rayonnement Synchrotron (DESIRS) beamline at SOLEIL. The resolving power of the measurements, $R = 300\,000$ to $400\,000$, allows the analysis of individual line strengths and widths within the bands. Gas column densities in the differentially pumped system were calibrated using the B-X (0–0) band at 115.1 nm in $^{13}C^{18}O$.

Key words. ISM: molecules – methods: laboratory: molecular – molecular data – techniques: spectroscopic – ultraviolet: ISM

1. Introduction

Accurate values of molecular transition probabilities are needed for applications such as column density determinations in astrophysics, modelling of molecular photochemical processes, photofragment population determinations, lifetime calculations, and for assessing the validity of ab initio calculations. This work is part of a larger effort to catalogue, interpret, and model the photoabsorption and the photodissociation spectrum of CO. In the presence of a strong ultraviolet field, the primary destruction mechanism for interstellar and circumstellar CO and its isotopologues is photodissociation, which is entirely governed by discrete line absorption into predissociating levels in the wavelength range from 111.6 nm (first dissociation limit of CO) to 91.2 nm (ionization limit of atomic hydrogen). Because the photodissociation of CO is a line process, it is subjected to self shielding, which is an isotope selective effect, where the less abundant isotopologues of CO are self shielded to a lesser degree than $^{12}C^{16}O$ and thus have the highest photodissociation rates at most depths in a cloud. Accurate modelling requires basic quantitative spectroscopic data for $^{12}C^{16}O$ and other isotopologues at wavelengths below the dissociation limit. The data reported here are essential to accurate modelling of CO in far ultraviolet (FUV)-active astrochemical environments.

At wavelengths longward of 100 nm, transitions to low v vibrational levels of the first Rydberg states in the series converging to the CO^+ $X^2\Sigma^+$ state are preponderant, namely the $B^1\Sigma^+$ state (with a 3sσ Rydberg electron) and $C^1\Sigma^+$ (3pσ), and $E^1\Pi$ (3pπ) states. These have been recently studied in detail (Stark et al. 2014). Shortward of 100 nm the spectrum becomes progressively more congested and complex as additional excited states are accessed. The strongest transitions involve higher Rydberg states converging to the CO^+ ground state and the CO^+ $A^2\Pi$ excited state. Line strengths and linewidths are strongly affected by isotopic substitution (Lefèbvre-Brion & Majumder 2015; and Eidelsberg et al. 2016).

Recent work by our group has extended earlier studies and provided comprehensive sets of data concerning absorption

and photodissociation cross sections and the spectroscopy of Rydberg states, as well the valence $A^1\Pi$ state of CO and isotopologues (Eidelsberg et al. 2012, 2014; Gavilan et al. 2013; Stark et al. 2014; Heays et al. 2014; and Lemaire et al. 2015). Overviews and discussion of the spectroscopy in the 91.2–111.8 nm region for CO and both isotopic species $^{13}C^{16}O$ and $^{12}C^{18}O$ have been previously reported (Eidelsberg et al. 2012, 2014).

The present study provides high resolution measurements of oscillator strengths (f-values) and upper level predissociation rates for transitions: (a) to the four lowest vibrational levels of the $3s\sigma^1\Pi$ (W) state (built on the CO^+ $A^2\Pi$ core); and (b) to the $v = 2$ levels of the $4p\pi$ and $4p\sigma$ states and the $v = 0$ levels of the $5p\pi$ and $5p\sigma$ states (built on the CO^+ $X^1\Sigma^+$ core). This work completes our recent work on $^{12}C^{16}O$, $^{13}C^{16}O$, and $^{12}C^{18}O$ spectra for the same transitions obtained in the same experimental conditions.

For the Rydberg transitions we are following the notations of Eidelsberg et al. (1992). The $4p\pi$ electronic state has sometimes been labelled L, in particular the $v' = 0$ and 1 levels in Eidelsberg et al. (1992).

2. Experimental setup

Absorption spectra of the molecular isotopic species $^{13}C^{18}O$ were recorded in the 91–116 nm range using the VUV-FTS that is installed as a permanent end station on the DESIRS beamline at the SOLEIL synchrotron facility. An extended description of its specific use for CO measurements was presented in Eidelsberg et al. (2012). The characteristics of the DESIRS beamline and the spectrometer were described elsewhere (de Oliveira et al. 2009, 2011; Nahon et al. 2013).

The beamline undulator provides a coherent continuum background with a Gaussian-like profile of 7 nm typical bandwidth at 100 nm. Two overlapping spectral windows were employed in the present measurements to cover the analyzed wavelength range of 91–98 nm. A third window centred on the B-X (0–0) band at 112 nm was systematically used for column density calibration.

High purity $^{13}C^{18}O$ gas (Cambridge isotopes, ^{13}C: 99%, ^{18}O: 95%) continuously flowed through a 10 cm long and 1.2 cm diameter windowless absorption cell. Spectra were recorded at multiple column densities between 8 and 200×10^{14} cm^{-2} in order to observe both strong and weak lines. To avoid optical depth effects for the strongest bands, only measurements corresponding to an optical depth less than 1.5 (absorption depths less than 78%) were used in the fitting procedure. Most spectra were recorded at room temperature (295 K) but several were obtained with a windowless cell cooled by liquid nitrogen to a temperature of 90 ± 5 K. In a few cases, a supersonic pulsed jet spectrum at 15 K previously obtained at lower resolution (Rostas et al. 1994) was used in order to disentangle the regions where the lines are congested in the band heads or overlapped at high J values in room temperature spectra.

Owing to the strict linearity in the wavenumber scale, the spectra can be put on an absolute scale using a single reference line. The presence of an Ar I line with reference wavelength 89.4414 nm from the NIST (National Institute of Standards and Technology) Atomic Database (Salomon 2004) is used to improve the accuracy of the wavelength calibration by setting all the scans on the same wavelength scale. While the maximum resolution of the VUV-FTS is 0.08 cm^{-1}, signal-to-noise (S/N) and measurement duration considerations dictated a resolution of 0.32 cm^{-1} for most scans.

In summary the VUV-FTS provides a typical measured resolving power of 350,000 in the 90 to 125 nm range. Over the course of about one hour of data collection, 100 co-added scans resulted in an S/N at the peak of the undulator bandpass of ~60. The resulting spectral resolution results in an instrumental sinc function with full-width half-maximum (FWHM) of 4.0×10^{-4} nm at 115 nm and 2.8×10^{-4} nm at 93.1 nm.

Our absolute column densities in the windowless cell were determined for each external pressure setting by recording the B-X (0–0) absorption band (hereafter called B00) for which an accurate f-value of 0.0065 is known with 6% uncertainty by combining the results of Stark et al. (1999) and Federman et al. (2001) for $^{12}C^{16}O$. This value was adopted for $^{13}C^{18}O$ (and previously for $^{13}C^{16}O$ and $^{12}C^{18}O$). To test the possibility of an isotopologue dependence in the B-X (0–0) f-value, Stark et al. (2014) used the parameters of the coupled electronic states model for the B and D′ states developed by Tchang Brillet et al. (1992) to calculate the predicted changes in the f-value due to a small shift in the B00 term values. Stark et al. found that the model predicts a 1.7% difference between the lightest $^{12}C^{16}O$ and the heaviest $^{13}C^{18}O$ isotopologue, significantly smaller than our experimental uncertainties.

The f-values for each band were independently measured from at least three spectra recorded over a range of column densities and temperatures, and in all cases we found agreement within 10%. This provides an estimate of the possible systematic f-value uncertainty introduced by model-dependent assumptions, small pressure variations during spectral acquisition, or mechanical vibrations in the FTS which can slightly affect the measured intensity baseline (Heays et al. 2011). The total spread of measured f-values for each band was added in quadrature to the uncertainty of the reference B00 f-value to infer the systematic uncertainty associated with our measurements. The uncertainties quoted in the tables below included these systematic effects and statistical uncertainties, also taken in quadrature.

The various observed bands display a J dependence of their linewidths and/or have different widths associated with e- and f-parity levels of the upper state, which we often represent by a simple polynomial in $J(J+1)$. While the f-values and linewidths of some bands show a nearly unperturbed behaviour, others exhibit extreme departures from the unperturbed patterns. Most lines are at least partially blended and there is significant overlap between P and Q branch lines.

3. Analysis method

The fitting procedure used to determine the oscillator strengths of the $^{13}C^{18}O$ absorption bands has been previously described and recently applied to the absorption spectra of $^{12}C^{16}O$ and the two isotopologic species $^{13}C^{16}O$ and $^{12}C^{18}O$ under the same experimental conditions as used in the present study. Here we provide a brief summary.

In the data reduction, the transmitted intensity $I(\lambda)$ is related to the measured absorption cross section $\sigma_{\rm exp}$ through application of the Beer Lambert law

$$\sigma_{\rm exp}(\lambda) = (1/N)\ln[I_0(\lambda)/I(\lambda)]. \quad (1)$$

Here, $\sigma_{\rm exp}$ is the absorption cross section which includes the effect of finite instrumental resolution (reducing the apparent peak cross section of sharp lines), N is the column density, $I_0(\lambda)$ is the background continuum level, and $I(\lambda)$ is the transmitted intensity.

For each band, a simulated absorption cross section (σ) is first calculated from the position, strength, and predissociation

linewidth of each rotational line. The model generates a summed cross section by adopting a Voigt profile for each line composed of a Lorentzian width and Gaussian Doppler broadening. The predissociation widths are described by the Lorentzian FWHM, and at room temperature the Doppler width is 0.23 cm^{-1}. The summed cross section is converted into a transmission spectrum according to the Beer Lambert formula and convolved with a sinc function to reproduce the instrumental broadening of the spectrometer. This calculated spectrum is adjusted to best match the experimental spectra in a non-linear least squares fitting procedure.

For some measured bands, the rotational line f-values follow the simple pattern associated with unperturbed transitions and a temperature-dependent Boltzmann distribution of ground state rotational levels. For unperturbed $^1\Sigma - ^1\Sigma$ and $^1\Pi - ^1\Sigma$ transitions, the band oscillator strength, f, is related to rotational line strengths, $f_{J'J''}$, by:

$$^1\Sigma - ^1\Sigma \qquad f = (2J'' + 1) f_{J'J''}/S_{J'J''} \tag{2}$$

$$^1\Pi - ^1\Sigma \qquad f = 2(2J'' + 1) f_{J'J''}/S_{J'J''} \tag{3}$$

where $S_{J'J''}$ is the Hönl-London factor. For unperturbed bands, the band f-values derived from application of Eqs. (2) and (3) are independent of the rotational quantum number J and a single band f-value is used by the fitting procedure indicated above to describe an entire absorption band. When the line f-value pattern deviates significantly from those predicted by Hönl-London factors for the R, P, and Q branches due to perturbations, the band f-values, determined by fitting the strengths of well-resolved rotation lines independently, are characterized by a marked J dependence. The derived f-values are then fitted to a polynomial in $J'(J' + 1)$; the extrapolation to $J' = 0$ is referred as a rotationless band f-value denoted $f(0)$, where $f(x)$ refers to $x = J'(J' + 1)$.

Most of the bands display a J dependence of their natural (Lorentzian) linewidths and/or different linewidths associated with transitions to the e- and f-parity levels of the upper state. The J dependence of these linewidths are represented by simple polynomial fits in $J'(J' + 1)$. Predissociation rates, k, must be calculated from the measured natural (Lorentzian) linewidths Γ_L of the rotational transition, from the relation (Eidelsberg et al. 2006):

$$k(s^{-1}) = \Gamma_L (1000/\lambda)^2 \times 1.885 \times 10^{10},$$

with Γ_L at FWHM (in mÅ) and where λ (in Å) is the wavelength of the band origin for the transition. The predissociation rates k_e and k_f calculated for e- and f-parity levels, respectively, are represented by simple polynomial fits in $J'(J' + 1)$.

4. Results

4.1. $W\,^1\Pi - X^1\Sigma^+$ bands

An irregular progression of four red degraded and partially diffuse strong bands appears in the 92.5–97.4 nm range. These bands have been previously observed at lower resolution as transitions from the v'' fundamental to the $v' = 0, 1, 2, 3$ vibrational levels of the $3s\sigma$ core-excited singlet $^1\Pi$ Rydberg W state and are labelled W00, W10, W20, and W30 respectively (Eidelsberg et al. 2004). The intensities of these bands are well described by Hönl-London factors, and a single f-value is specified for each of the four bands. The four bands display J-dependent linewidths and/or different widths associated with the e- and f-parity levels in the upper state. A new set of wavelengths for W00 as well as for the W10 and W20 bands has been measured from our SOLEIL spectra and recently published (Lefèbvre-Brion & Eidelsberg 2012). A complete listing may be obtained from the corresponding author upon request.

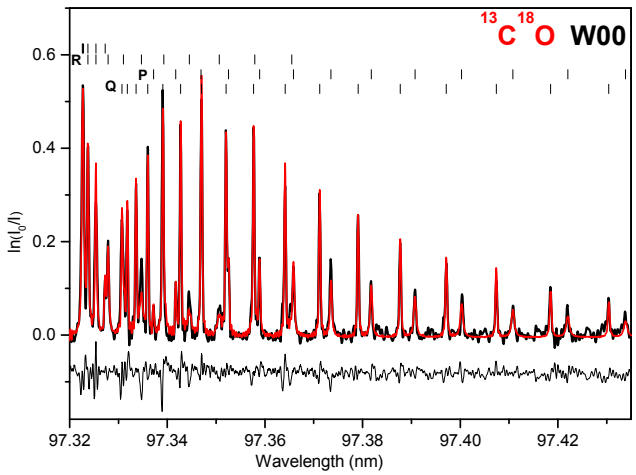

Fig. 1. $^{13}C^{18}O$ W($v = 0$) – X(0) band experimental absorption spectrum (black lines) and fit (red lines). The fitting residuals are shifted by 0.08.

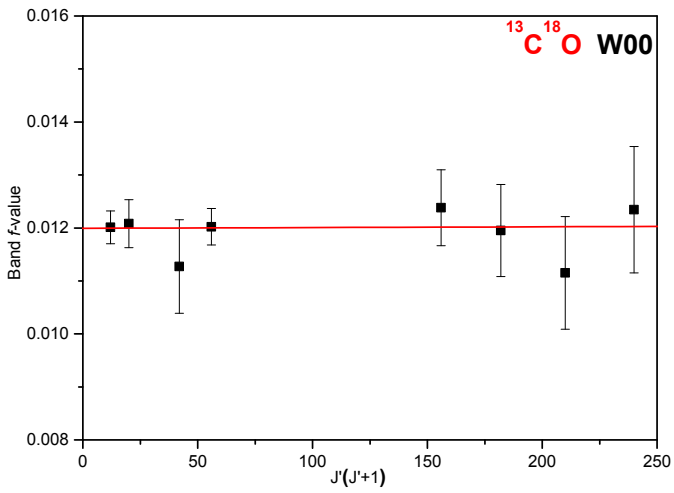

Fig. 2. $^{13}C^{18}O$ Q branch oscillator strength for the W($v = 0$) – X(0) band.

4.1.1. W00

The origin of this band is slightly shifted to the red relative to the other isotopologues we have studied, despite being a $v = 0$ state. Our wavelength measurements are in good agreement but slightly more precise than the published values of Eikema et al. (1994) obtained with a tunable source with an accuracy of 0.13–0.3 cm^{-1}. The P- and R-branch lines observed at higher J' values than in the Eikema spectra exhibit distinct line broadening accompanied by a sharp drop in intensity, whereas the Q lines remain narrow and their intensities follow Hönl-London factors for a room temperature spectrum until high J' values. A single band oscillator strength is obtained by fitting the R, P, and Q branch lines together (Fig. 1). The band oscillator strength derived from fitting individual resolved Q lines was found to be independent of J' (Fig. 2).

The Lorentzian linewidths, Γ_l, fitted to the resolved Q-branch lines are approximately constant or gradually increasing until $J' = 14$, while the P branch linewidths show a rapid increase

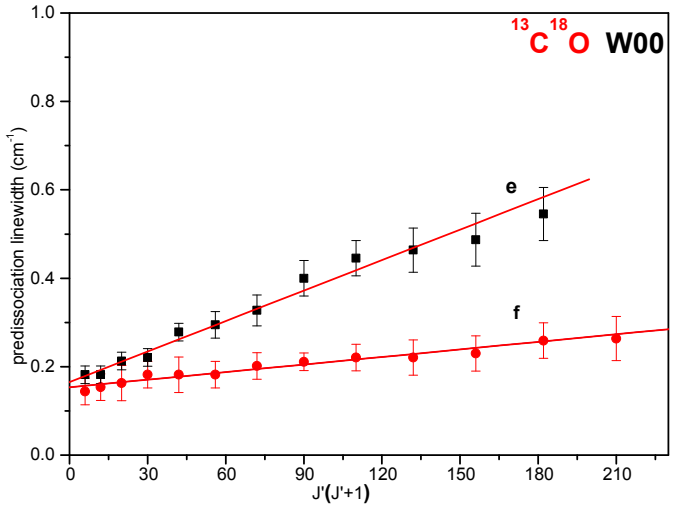

Fig. 3. $^{13}C^{18}O$ predissociation linewidth for the W(v = 0) – X(0) band (widths are shown for e- and f-parity levels).

with J' (Fig. 3). The predissociation linewidths for e and f components were then fitted to separate functions.

4.1.2. W10

The W10 band was studied by our team and results obtained at the SOLEIL Synchrotron for five isotopologues, $^{12}C^{16}O$, $^{12}C^{17}O$, $^{13}C^{16}O$, $^{12}C^{18}O$, and $^{13}C^{18}O$, were recently published (Heays et al. 2014). The results obtained for the $^{13}C^{18}O$ isotopologue are completed here.

The calculated absorption spectrum $\ln(I/I_0)$ obtained between 95.58 and 95.76 nm from the Fourier transform spectrometer for column densities of 1.48×10^{15} cm^{-2} at room temperature is reproduced in Fig. 4a. A predissociation broadened red degraded feature overlaps the high rotational lines of this spectrum which is not observed in the other CO variants. The W10 band and this feature are well separated on the jet absorption spectrum obtained at 15 K with the ten meter spectrograph in Meudon (Rostas et al. 1994) at lower resolution (Fig. 4b). To obtain an isolated spectrum of the W10 band, an unresolved red degraded feature of a band of $\Pi - X$ profile is first subtracted from the calculated spectrum $\ln(I/I_0) = f(\lambda)$. After several iterations of adjusting the profile of the $\Pi - X$ band, a simulated spectrum of the W10 band is calculated to best match the absorption spectrum (Fig. 5).

As for the $^{12}C^{16}O$, $^{13}C^{16}O$, and $^{12}C^{18}O$ isotopologues, the W10 band is broadened and has blended rotational lines. Thus, few oscillator strengths and widths could be fitted independently. The Lorentzian predissociation linewidth is found to be parity independent (Fig. 6) in good agreement with the natural linewidths of Fig. 6 in Heays et al. (2014). These widths show a sudden decrease between J = 7 and 8; a similar phenomenon for the $^{12}C^{16}O$ isotopologue was quantitively modelled by Lefèbvre-Brion & Kalemos (2016) as the result of a multistate interaction of bound and dissociative states.

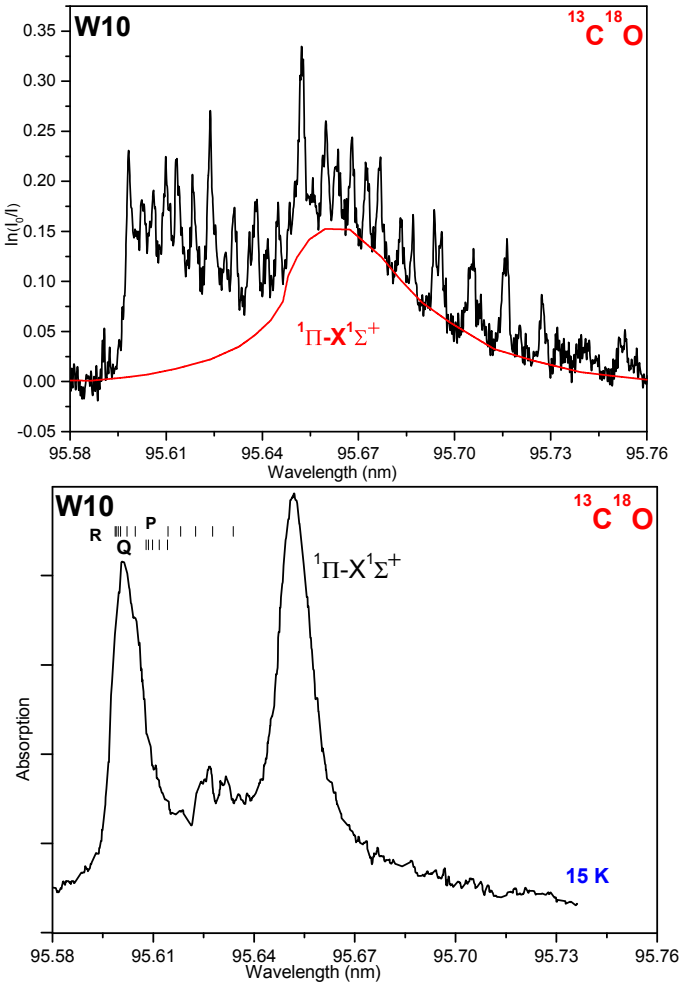

Fig. 4. **a)** (*upper*) $^{13}C^{18}O$ W(v = 1) – X(0) band experimental spectrum (black lines) and profile of the unknown $\Pi - X$ band (in red). **b)** (*lower*) $^{13}C^{18}O$ absorption spectrum at low temperature (Rostas et al. 1994).

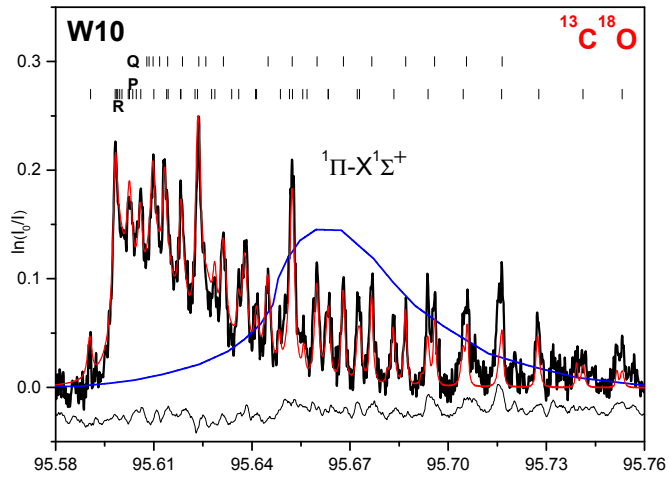

Fig. 5. $^{13}C^{18}O$ W(v = 1) – X(0) band experimental absorption spectrum (black lines), and fit (red lines) and unknown band profile (blue). The fitting residuals are shifted by 0.04.

4.1.3. W20

The rotational line strengths of the W20 band are well characterized by Hönl-London factors. Local perturbations observed in $^{13}C^{16}O$ and $^{12}C^{18}O$ were not detected. A fit of this band is reproduced in Fig. 7. The predissociation effects are found to be parity independent and the linewidth Γ_L of the R, P, and Q lines follows a similar trend and must be fitted by a polynomial curve reproducing a rapid increase in the predissociation linewidths from $J' = 7$ (Fig. 8).

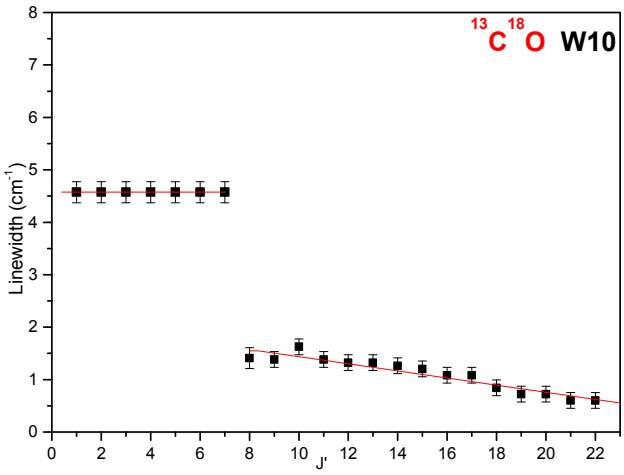

Fig. 6. $^{13}C^{18}O$ predissociation linewidth for the W(v = 1) – X(0) band.

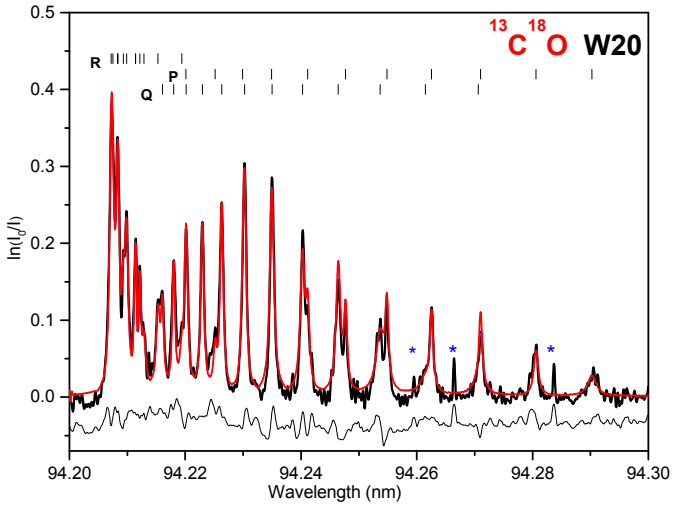

Fig. 7. $^{13}C^{18}O$ W(v = 2) – X(0) band experimental absorption spectrum (black lines) and fit (red lines). The fitting residuals are shifted by 0.05. Blue stars show N_2 impurity lines at 94.2595, 94.2663, and 94.2837 nm.

4.1.4. W30

The band head of the W30 R branch is heavily blended and only a few R lines with high J' values were identified, mixed in with low-J' Q lines. The P and Q lines are partially blended but easily identified until J' = 14 (Fig. 9). Some of them are resolved and were analyzed independently. The predissociation rates were determined by fitting the entire band with a J-independent band oscillator strength and a set of predissociation linewidths with assumed separate J dependence for e- and f-parity levels. The linear J dependence of predissociation linewidths assumed during the fitting process is shown in Fig. 10.

4.1.5. Summary

The deduced f-values for four W-X bands are reported in Table 1, along with results from previous measurements obtained at lower resolution (Eidelsberg et al. 1991; Eidelsberg et al. 2006). The published results for the four bands by Eidelsberg et al. (1991) were obtained by isotopic extrapolation. Improvement by a factor of ten in spectral resolution over data obtained previously at SuperACO (Eidelsberg et al. 2006) allowed us to measure linewidths with higher accuracy. Our f-value results for

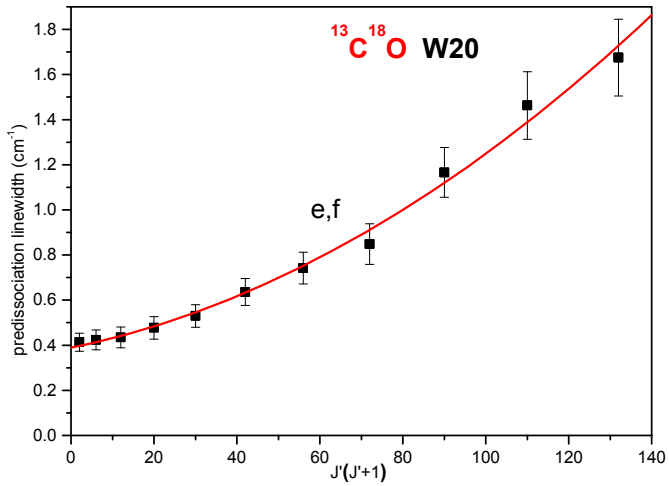

Fig. 8. $^{13}C^{18}O$ predissociation linewidth for the W(v = 2) – X(0) band.

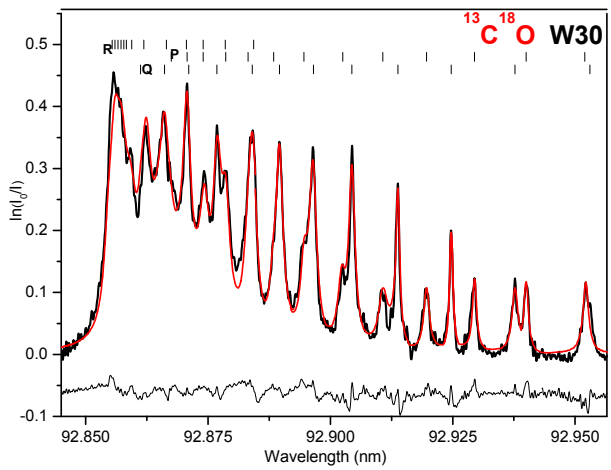

Fig. 9. $^{13}C^{18}O$ W(v = 3) – X(0) band experimental absorption spectrum (black lines) and fit (red lines). The fitting residuals are shifted by 0.06.

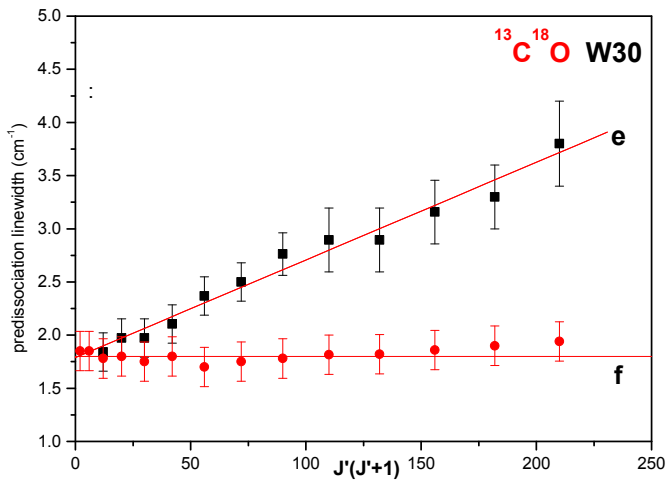

Fig. 10. $^{13}C^{18}O$ predissociation linewidth for the W(v = 3) – X(0) band.

the W bands are generally lower than these earlier values, but are within the 1σ mutual uncertainties except for the W00 band, where agreement is at the 2σ level. In light of this correspondence, we provide weighted averages for the W00, W20, and W30 in the last column of Table 1. The W10 band mixed with

Table 1. f-values ($\times 10^{-3}$) for W band and the unknown band overlapping W10.

Band	λ_0(nm)	Present	E06	E91	WA*
W00	97.329	11.6(0.8)	13.8(2.0)	13.2(1.3)	12.2(0.6)
W10	95.604	7.0(0.7)		16.0(1.6)	
$^1\Pi - X(v', 0)$		5.7(0.8)			
W20	94.24	22.9(1.8)	28.5(2.0)	27.9(2.8)	25.9(1.2)
W30	92.86	13.8(1.1)	15.4(2.4)	18.6(1.9)	15.0(0.9)

Notes. Comparison with previous results: E91 (Eidelsberg et al. 1991), E06 (Eidelsberg et al. 2006). (*) Weighted average.

Table 2. Predissociation rates for W bands in units of 10^{11} s^{-1}, with $X = J'(J'+1)$.

Band	Ref	k_e	k_f
W00	Present	0.320(0.026)+0.0036(0.0008)X	0.266(0.021)+0.0013(0.0003)X
	E06	0.11(0.01)+0.01(0.01)X	
	Eikema	<0.3 for $J \leq 15$	
W10	Present	8.60(0.37) $J' = 0$ to $J' \leq 8$	
		4.13(0.19)–0.130(0.017)X $J' > 8$	
W20	Present	0.733(0.053)+0.0074(0.0023)X + 9.0(2.0) $\times 10^{-5} X^2$	
	E06	0.42(0.06)+0.038(0.017)X	0.42(0.06)+0.021(0.010)X
W 30	Present	3.43(0.26)+0.173(0.021)X	3.41(0.34)
	E06	4.4	

Notes. Rates are given for e- and f-parity levels. Comparison with previous results: E06 (Eidelsberg et al. 2006) and Eikema et al. (1994).

the new $^1\Pi - X^1\Sigma^+$ band was not resolved on the SuperACO spectra, but the sum of the f-values is more or less consistent with our previous measurements (Eidelsberg et al. 1991).

Table 2 provides a comparison between our predissociation rates (k_e and k_f) and those of Eikema et al. (1994) and Eidelsberg et al. (2006). The former are based on laser measurements. The results are in rough agreement, within a factor of two of those quoted by Eidelsberg et al. (2006) and less than or approximately equal to the upper limits found by Eikema et al. (1994). The lower spectral resolution in our earlier measurements is the likely cause for the factor of two differences in the narrower lines.

4.2. 4p and 5p complexes

The absorption spectrum between 93.2 and 93.4 nm is more congested (as shown in Fig. 19) in this isotopologue than those we have previously studied. The three bands $4p\pi^1\Pi - X^1\Sigma^+$(2–0), $5p\pi^1\Pi - X^1\Sigma^+$(0–0), and $5p\sigma^1\Sigma^+ - X^1\Sigma^+$(0–0) are well resolved in $^{13}C^{16}O$ and $^{12}C^{18}O$, but overlapped at room temperature for $^{13}C^{18}O$ (Fig. 11a). The identification of rotational lines was facilitated by recording a high resolution spectrum taken at high pressure while cooling with liquid N_2 to 90 K (Fig. 11b) and a very cold spectrum obtained at 15 K at lower resolution with a pulsed supersonic free jet (Fig. 11c) (Rostas et al. 1994). This allows us to disentangle the spectrum and identify the three strongest bands (labelled in Fig. 11b). A weak band with optically thin lines appears at high pressure within the P branch of the $5p\sigma^1\Sigma^+ - X^1\Sigma^+$(0–0) band and we attribute this to the $4p\sigma^1\Sigma^+ - X^1\Sigma^+$(2–0) band which is expected to accompany the $4p\pi^1\Pi$ absorption. There is some additional continuum-like absorption occurring in the spectrum which is not necessarily attributable to the 4p5p complex of bands. This is indicated in Fig. 11a by the cross section component marked "I_c". A synthetic spectrum showing detailed assignments for the four bands associated with the two Rydberg complexes 4p and 5p is presented in Fig. 12 where the extra absorption I_c shown in Fig. 11a has been subtracted.

4.2.1. 4p(2) complex

4.2.1.1 $4p\pi^1\Pi - X^1\Sigma^+$ (2–0)

The spectrum of the $4p\pi^1\Pi - X^1\Sigma^+$ (2–0) band is well resolved and the R, P, and Q lines are best identifiable in the cold spectrum obtained at 90 K (Fig. 11b). The few R lines of the $5p\pi^1\Pi - X^1\Sigma^+$(0–0) band which appear within the P branch are sharp and easily identifiable. Simulated spectra calculated at room temperature were initially made using Hönl-London strength factors for a pure $^1\Pi - ^1\Sigma$ transition. The fit was applied to the part of the spectrum where there was no overlap with other bands, until $J = 8$ for Q lines and $J = 10$ for P lines (Fig. 13). Predissociation linewidths of the f component were measured until $J' = 13$. Only a few R and P linewidths could be measured for the e component (Fig. 14). The predissociation rate was found to be parity dependent and shows a linear dependence with $J'(J'+1)$.

4.2.1.2 $4p\sigma^1\Sigma^+ - X^1\Sigma^+$ (2–0)

A series of regular, narrow lines appears within the P branch of the $5p\sigma^1\Sigma^+ - X^1\Sigma^+$(0–0) band in the 90 K spectrum at high pressure (Fig. 11b), and can be attributed to the P branch of the $4p\sigma^1\Sigma^+ - X^1\Sigma^+$(2–0) band of the 4p(2) complex. These lines are very weak in the room temperature spectrum. The P branch is well observed until $J' = 12$ in the very high pressure cold spectrum at 90 K. The R(0) line at 93.306 nm is clearly identified

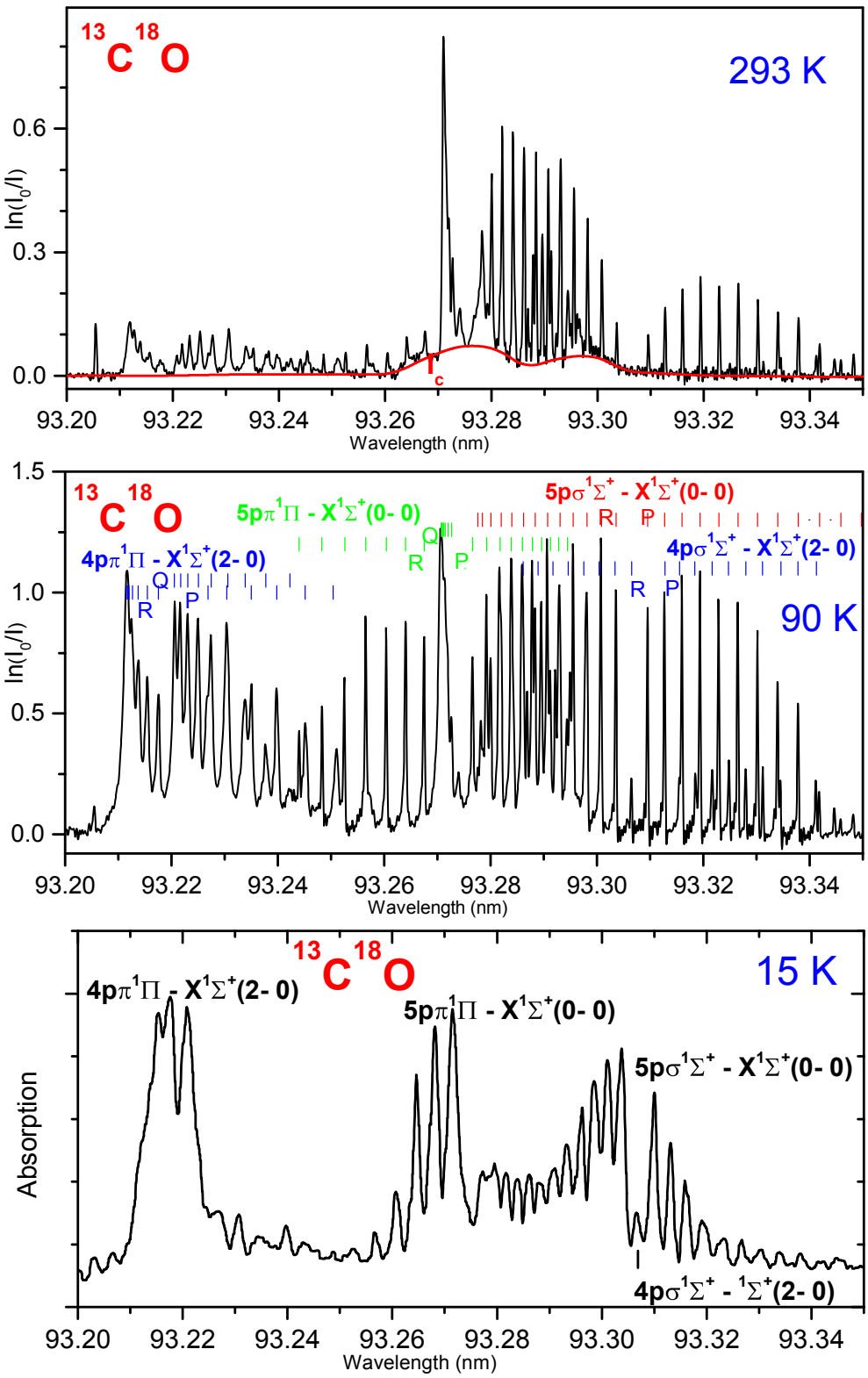

Fig. 11. **a)** Absorption spectrum at room temperature in the 93.20–93.35 nm range (profile of an unknown band in red) (*upper*). **b)** Absorption spectrum at 90 K in the 93.20–93.35 nm range (*centre*). **c)** Low resolution absorption spectrum at 15 K in the same range (Rostas et al. 1994) (*lower*).

in the spectrum at 15 K (Fig. 11c). Only a few *R* lines can be observed in the blended region of the *P* branch of the $5p\pi^1\Pi$ – $X^1\Sigma^+(0–0)$ band.

Line wavelengths for this new band are reported in Table 3. The band was fitted using line strengths that follow a Hönl-London distribution for a $^1\Sigma^+$ –$^1\Sigma^+$ transition following comparison of the simulated spectrum and the measured absorption spectrum. The f-value is found to be very small, $<2\times10^{-5}$.

4.2.2. 5p(0) complex

The $5p\pi^1\Pi$ – $X^1\Sigma^+(0–0)$ and $5p\sigma^1\Sigma^+$ – $X^1\Sigma^+(0–0)$ bands are clearly identified in the cold 15 K spectrum at low resolution

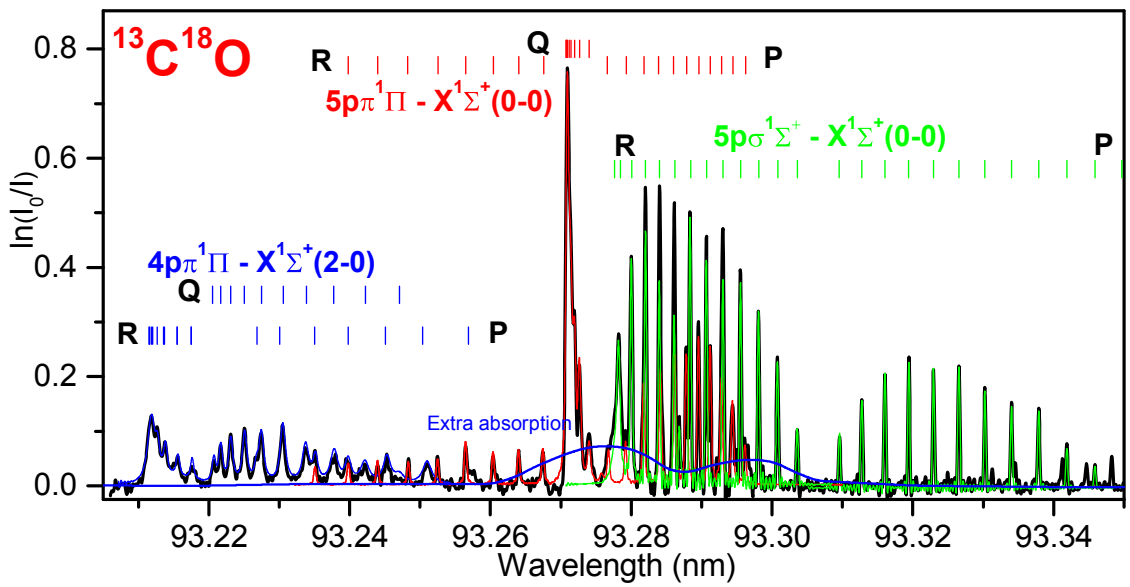

Fig. 12. $^{13}C^{18}O$ composite synthetic spectrum.

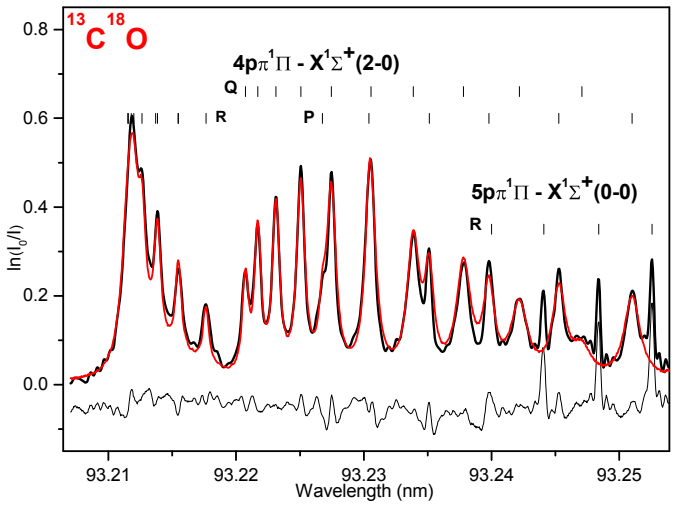

Fig. 13. $^{13}C^{18}O$ $4p\pi^1\Pi(v = 2) - X(0)$ band experimental absorption spectrum (black lines) and fit (red lines). The fitting residuals are shifted by 0.04.

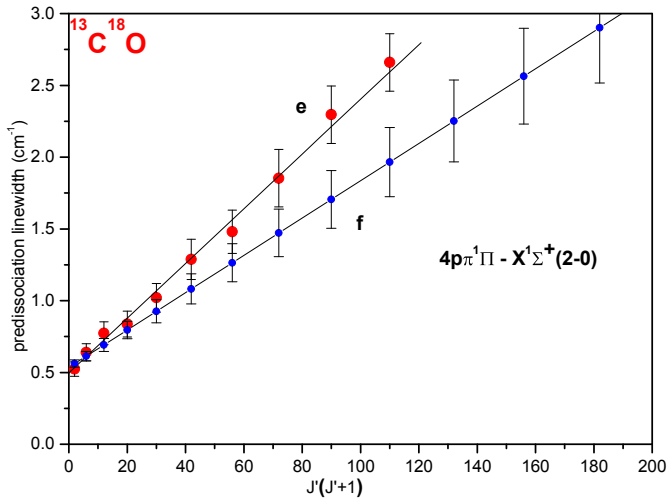

Fig. 14. $^{13}C^{18}O$ predissociation linewidth for the $4p\pi^1\Pi(v = 2) - X(0)$ band. An assumed linear fit for f-parity levels is shown, extrapolated with uncertainties given by the quality of the polynomial fit.

(Fig. 11c). There is significant overlap between the P branch of $5p\pi^1\Pi - X^1\Sigma^+(0–0)$ and the R branch of $5p\sigma^1\Sigma^+ - X^1\Sigma^+(0–0)$ at room temperature as well as at 90 K (Figs. 11a and b). The R branch lines of $5p\pi^1\Pi - X^1\Sigma^+(0–0)$, are partially mixed with the P and Q branches of $4p\pi^1\Pi - X^1\Sigma^+0–0)$ but they are sharp and easily identified.

4.2.2.1 $5p\pi^1\Pi - X^1\Sigma^+$ (0–0)

Rotational R lines are clearly seen in the 90 K spectrum and measured until $J' = 5$. Only a few P lines could be distinguished within the R branch of the $5p\sigma^1\Sigma^+ - X^1\Sigma^+(0–0)$ band in the 295 K spectrum. Most rotational Q lines are not resolved and only a few lines are assigned (Fig. 12).

At first, the entire $5p\pi^1\Pi - X^1\Sigma^+(0–0)$ band was simulated by assuming unperturbed Hönl-London factors. Line f-values thus calculated deviate significantly from those predicted by Hönl-London factors for a $^1\Pi - ^1\Sigma$ transition. The most striking feature

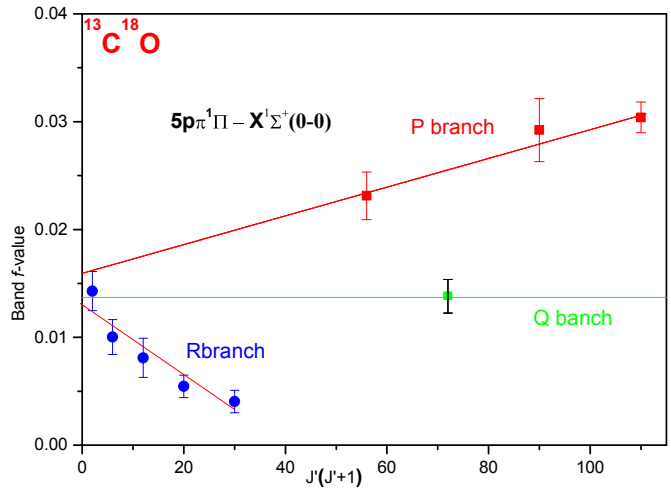

Fig. 15. $^{13}C^{18}O$ oscillator strength for the $5p\pi^1\Pi(v = 0) - X(0)$.

Table 3. Wavelengths (0.0001 nm uncertainty) of observed lines for $4p\sigma^1\Sigma^+ - X^1\Sigma^+(2–0)$ (nm).

P(1)	93.3122		
P(2)	93.3157	R(0)	93.3064
P(3)	93.3115		
P(4)	93.3185		
P(5)	93.3248		
P(6)	93.3280		
P(7)	93.3312		
P(8)	93.3345		
P(9)	93.3378		
P(10)	93.3412		
P(11)	93.3446		
P(12)	93.3488		

Table 4. Rotationless f-values for bands in the 4p5p region ($\times 10^{-3}$).

Band upper level	λ (nm)	Present*	E91
$4p\pi(2)$	93.217	9.6(0.9)	6.2(0.6)
$4p\sigma(2)$	93.311	<2	
$5p\pi(0)$	93.267	13.9(1.1)	
$5p\sigma(0)$	93.304	16.2(1.4)	16.8(1.7)
Extra-absorption	Between 93.245-93.315	9.2 (1.0)	

Notes. Comparison with previous results: E91 (Eidelsberg et al. 1991). (*) The present measurements are judged more reliable than those of E91 due to the possibility of misassignment of absorption in the earlier lower-resolution work. Then, no weighted average is provided.

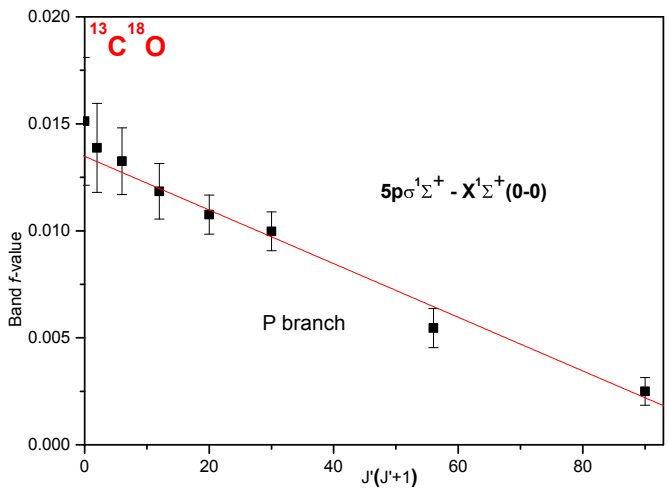

Fig. 16. $^{13}C^{18}O$ oscillator strength for the $5p\sigma^1\Sigma(v = 0) – X(0)$.

is the rapidly increasing strength of the P branch lines with increasing rotational quantum number and the relative weakness of the R branch lines at low J' values; the strength of the Q lines remains unperturbed. Consequently, a fitting procedure assuming a single f-value for the band was not ultimately used. An individual fit was calculated for each rotationally-resolved P, R, and Q branch line, providing information on the J dependence of the band oscillator strength (Fig. 15). The measured oscillator strengths and the band f-values derived from lines within the P, R, and Q branches converge to a common rotationless f-value of 13.9×10^{-2}, as shown in Fig. 15. This is consistent

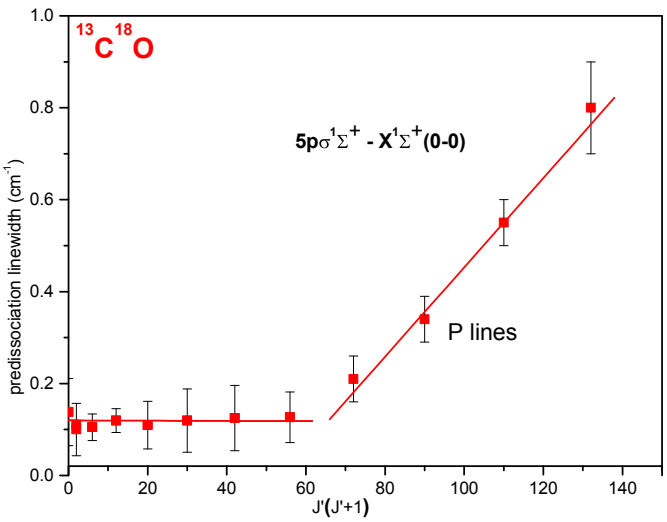

Fig. 17. $^{13}C^{18}O$ predissociation linewidth for the $5p\sigma^1\Sigma(v = 0) – X(0)$.

with rotational l-uncoupling mixing the $5p\pi^1\Pi$ and $5p\sigma^1\Sigma^+$ Rydberg levels for $J > 0$ and leading to mutual interference effects in their line strengths (Lefèbvre-Brion & Field 2004). A fit of the entire band with adjusted line intensities and widths, as determined by the fit of individual R and Q branch linewidths, is reported in Fig. 12. The linewidths measured for five R lines and three P lines are found to be slightly J dependent and the calculated linewidths for the e component are represented by a linearly-increasing function of $J'(J'+1)$. The linewidth has been measured only for one Q line at $J' = 8$. The modelled spectrum represented in Fig. 18 has been obtained using the same calculated linewidths for e and f components.

4.2.2.2 $5p\sigma^1\Sigma^+ – X^1\Sigma^+$ (0–0)

The same procedure used to determine oscillator strengths for $5p\pi^1\Pi – X^1\Sigma^+(0–0)$ was applied to the $5p\sigma^1\Sigma^+ – X^1\Sigma^+(0–0)$ band. The P branch of the $5p\sigma^1\Sigma^+ – X^1\Sigma^+(0–0)$ band is well developed until $J' = 12$ and the f-values for nine P lines were fitted to a linearly decreasing function of $J'(J'+1)$ (Fig. 16). The R branch lines are stronger than predicted by Hönl-London factors for a $^1\Sigma -^1 \Sigma$ transition, due to their intensity interference with $5p\pi^1\Pi – X^1\Sigma^+(0–0)$. The predissociation linewidths reported in Fig. 17 are small and approximately constant for $J' < 8$, and then increase gradually.

4.2.3. Extra continuum absorption

The origin of the continuum-like component, I_c, of the observed cross section is not completely clear but some observations may be made. The extra absorption only appears in the room temperature spectrum, and is not evident at 90 or 15 K, suggesting that transitions from high-J' rotational levels are responsible.

It is then possible that the absorption between 93.27 and 93.31 nm may be attributable to P- and Q-branch lines of $5p\pi^1\Pi – X^1\Sigma^+(0–0)$, and perhaps R-branch lines of $4p\sigma^1\Sigma^+ – X^1\Sigma^+(2–0)$. The strength of the extra absorption is broadly consistent with this hypothesis and its lack of rotational structure could be attributable to a continuing increase of predissociation widths above the assigned $5p\pi^1\Pi – X^1\Sigma^+(0–0)$ transitions leading to a pseudo-continuum of overlapped broadened lines.

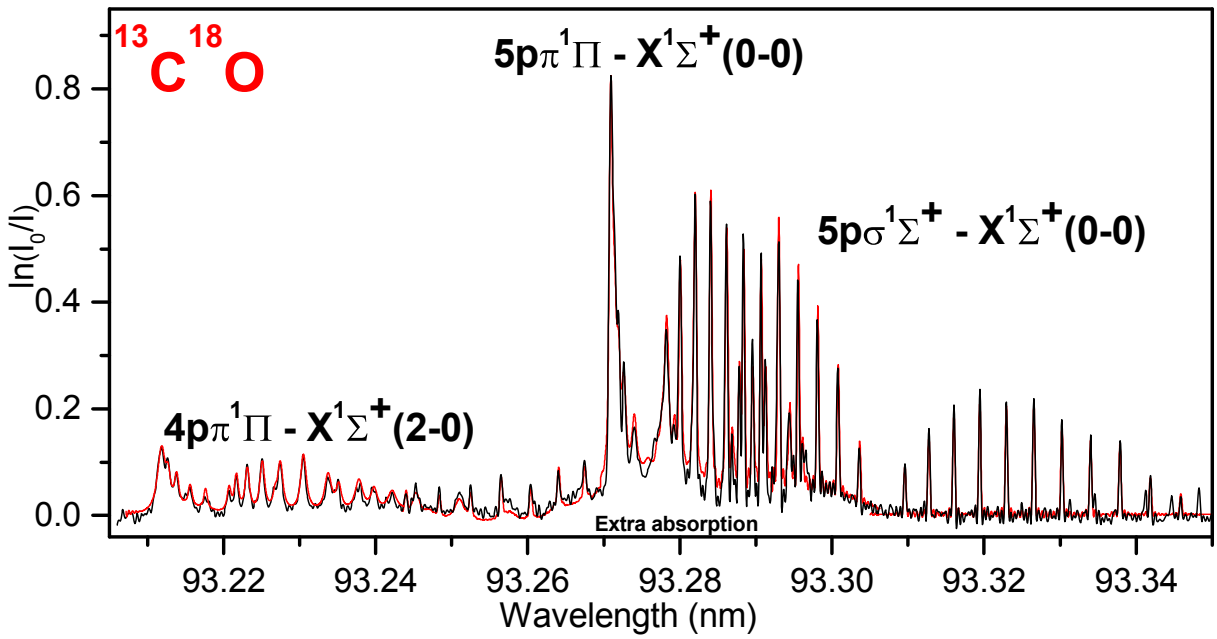

Fig. 18. $^{13}C^{18}O$ experimental and calculated spectra in the 93.2–93.36 nm range.

Table 5. Predissociation rates for bands in the 4p5p region (in units of 10^{11} s^{-1}), with $X = J'(J'+1)$.

Band upper level	Ref.	k_e	k_f
$4p\pi^1\Pi$ (2)	Present	0.90(0.11)+0.041(0.005)X	1.00(0.11)+0.024(0.003)X
	E91	1.0	
$5p\pi^1\Pi$ (0)	Present	0.54(0.11)+0.0011(0.0011)X	0.54(0.11) at $J = 8$
$5p\sigma^1\Sigma^+$ (0)	Present	$J' < 8$: 0.226(0.024); $J' > 7$: –0.978(0.098)+0.018(0.003)X	
	E91	0.1	

Notes. Rates are given for e- and f-parity levels. Comparison with previous results: E91 (Eidelsberg et al. 1991).

Table 6. Comparison of SOLEIL f-values ($\times 10^{-3}$) summed over each W-X band in various isotopologues with previous values E12 (Eidelsberg et al. 2012), E14 (Eidelsberg et al. 2014).

Band Upper level	Present $^{13}C^{18}O$	E12 $^{12}C^{16}O$	E14 $^{13}C^{16}O$	E14 $^{12}C^{18}O$
W(0)	11.6(0.8)	14.3(1.1)	12.67(0.82)	13.94(0.86)
W(1)	7.0(0.7)			
$^1\Pi(v')$	5.7(0.8)			
W(1)+$^1\Pi(v')$	12.7	17.5(1.3)	14.78(0.94)	13.37(0.83)
W(2)	22.9(1.8)	28.9(2.1)	27.14(1.72)	26.40(1.63)
W(3)	13.8(1.1)	19.2(1.4)	15.92(1.02)	18.10(1.12)

It does not appear feasible that the extra absorption between about 93.26 and 93.30 nm could arise from members of the 4p5p complex. However, a very similar feature appears in spectra of $^{13}C^{16}O$ and $^{12}C^{18}O$ (Eidelsberg et al. 2014) centred at 93.25 nm, and a clearly resolved $^1\Pi-^1\Sigma^+$ band was observed near 93.15 nm in $^{12}C^{16}O$ (Eidelsberg et al. 2012). We intend to investigate these features further with a multi-isotopologue analysis.

4.2.4. Final results

Measured and simulated spectra of five bands observed between 93.2 and 93.35 nm are shown in Fig. 12. Modelled and experimental spectra are compared in Fig. 18. All deduced f-values and predissociation rates are listed in Tables 4 and 5, including results for the extra absorption I_c in the 93.26 and 93.30 nm range. Comparisons are made with previous results (Eidelsberg et al. 1991) obtained at low resolution (R = 30 000). The few corresponding measurements show good agreement.

5. Concluding remarks

Spectra showing absorption into the $W^1\Pi$ (v = 0–3) levels and 4p(v = 2) and 5p(v = 0) Rydberg series converging to the CO^+ ground state, $X^1\Sigma^+$, are shown in Fig. 19 for the isotopic species $^{12}C^{16}O$, $^{13}C^{16}O$, and $^{13}C^{18}O$ ($^{12}C^{18}O$ is omitted as it is very similar to $^{13}C^{16}O$). All these spectra were obtained under the same experimental conditions. Tables 6 and 7 show our complete set of measured f-values for the observed absorption bands for $^{13}C^{18}O$ (this work), $^{12}C^{16}O$ (Eidelsberg et al. 2012), and $^{13}C^{16}O$ and $^{12}C^{18}O$ (Eidelsberg et al. 2014). Related details for the W10 band

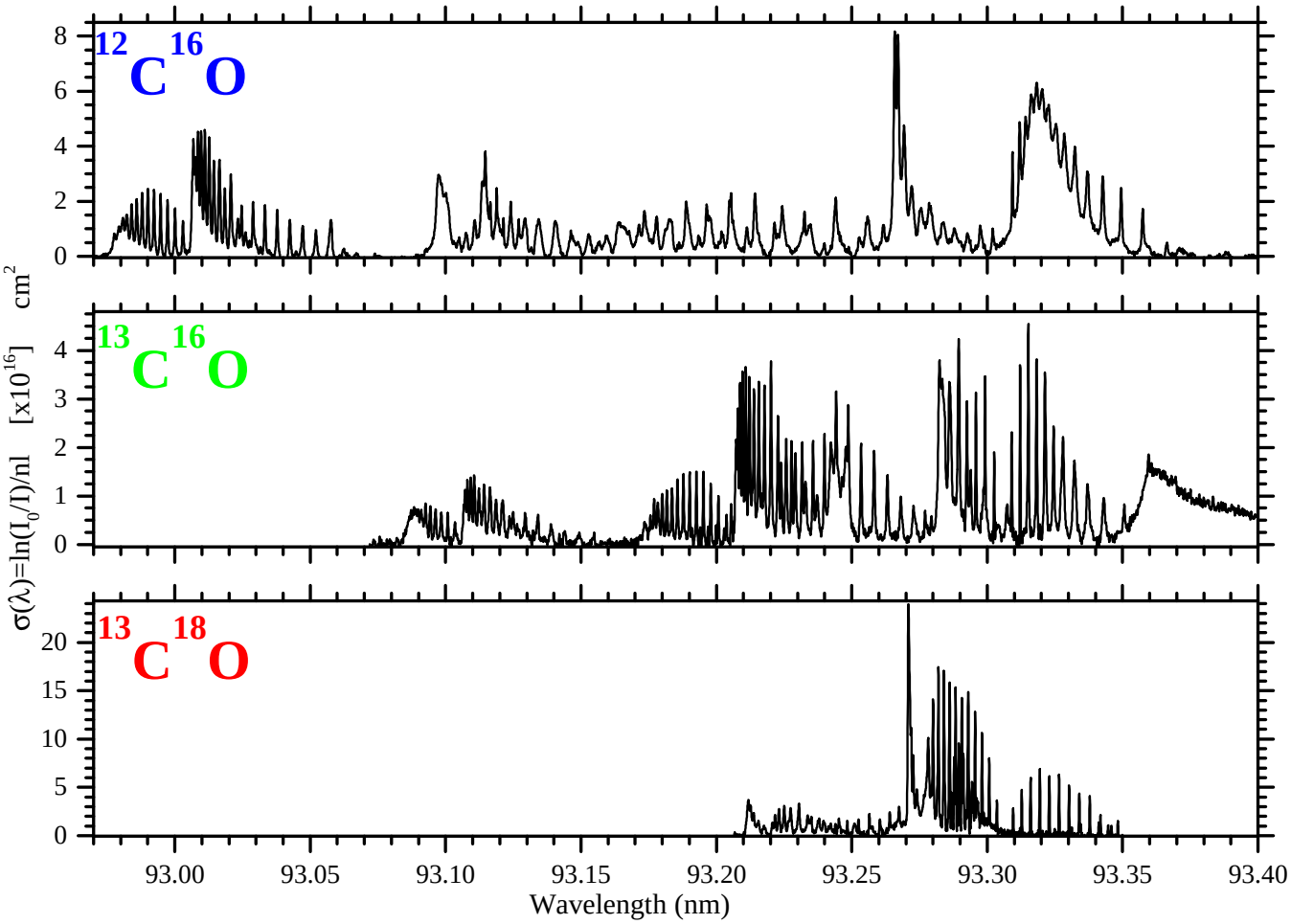

Fig. 19. Cross section comparison of the 4p(2) and 5p(0) experimental spectra for $^{12}C^{16}O$ (*top*, E12), $^{13}C^{16}O$ (*middle*, E14), and $^{13}C^{18}O$ (*bottom*, this work), at the same wavelength scale.

Table 7. Comparison of SOLEIL rotationless f-values ($\times 10^{-3}$) summed over each band in the 4p5p region in various isotopologues with previous values, E12(Eidelsberg et al. 2012), E14 (Eidelsberg et al. 2014).

Band Upper level	Present $^{13}C^{18}O$	E12 $^{12}C^{16}O$	E14 $^{13}C^{16}O$	E14 $^{12}C^{18}O$
4pπ(2)	9.6(0.9)	8.01(0.56)	6.19(0.44)	6.81(0.48)
II $^1\Pi$	*	5.96(0.52)	2.1(0.2)	2.8(0.3)
4pσ(2)	<0.02	0.99(0.11)	1.0(0.2)	
5pπ(0)	13.9(1.1)	9.30(0.88)	13.55(1.03)	15.99(1.26)
5pσ(0)	16.2(1.4)	14.6(1.0)	13.68(0.96)	15.63(1.21)
I $^1\Pi$	*	4.67(0.84)	11.0(0.9)	15.55(1.24)
Extra absorption**	9.2(1.0)	14.5(1.3)		
4p5p sum	**48.9(4.4)**	**58.0(5.2)**	**47.6(3.5)**	**56.8(4.5)**

Notes. (*) Not observed in $^{13}C^{18}O$. (**) The extra absorption f-value is not rotationless but instead calculated as a pseudo-band f-value from the integrated cross section at room temperature.

in all isotopologues can be found in Heays et al. (2014). This suite of measurements represents the most complete database available for these transitions. The same applies to the measured predissociation rates. Our larger set of measurements provides J-dependent rates (Table 8 and 9).

Our measurements are especially useful for chemical models that incorporate details of CO photodissociation. Oscillator strengths and predissociation rates are now available to examine selective isotope photodissociation with greater precision. We note that the significant linewidths for most of the W10 band minimize the importance of these transitions to selective self-shielding, where the most abundant forms of CO are protected from dissociation, because optical depths at their line centres cannot reach large values. In general, self-shielding in

Table 8. Comparison of SOLEIL predissociation rates for W bands in various isotopologues (in units of $10^{11} s^{-1}$), with $X = J'(J'+1)$.

Band	Predissociation rates (10^{11} s^{-1})	
Isotopologue	*e*-parity	*f*-parity
W00		
$^{12}C^{16}O^a$	0.09(0.02)+0.019(0.001)X	0.10(0.01)+0.0016(0.0001)X
$^{13}C^{16}O^b$	0.220(0.060)+0.011(0.001)X	0.187(0.009)+0.002(0.001)X
$^{12}C^{18}O^b$	0.226(0.021)+0.0147(0.0004)X	0.228(0.009)+0.00130(0.00007)X
$^{13}C^{18}O$	0.320(0.026)+0.0036(0.0008)X	0.266(0.021)+0.0013 (0.0003)X
W10		
$^{12}C^{16}O^a$	$J' > 6$: 1.87(0.53)+ 3.3(0.017)X	
$^{13}C^{16}O^b$	$J' < 8$: 2.92(0.15)+0.102(0.006)X; $J' > 7$: -4.77(0.24)+0.081(0.009)X	
$^{12}C^{18}O^b$	$J' < 8$: 1.87(0.53)+0.141(0.01)X; $J' > 7$: –5.96(0.60)+0.094(0.004)X	
$^{13}C^{18}O$	$J' < 8$: 8.60(0.40); $J' > 7$: 4.13(0.19)−0.130(0.017)X	
W20		
$^{12}C^{16}O^a$	1.12(0.05)+0.010(0.001)X	0.75(0.04)+0.0060(0.0002)X
$^{13}C^{16}O^b$	0.472(0.043)+0.0067(0.0011)X+[9.4(0.6)]$10^{-5}X^2$	
$^{12}C^{18}O^b$	0.644 (0.004)+0.00170(0.0009)+[5.27(0.35)]$10^{-5}X^2$	
$^{13}C^{18}O$	0.733(0.053)+0.0074(0.0023)X +9.0(2.0)$X10^{-7}X^2$	
W30		
$^{12}C^{16}O^a$	2.07(0.10)+0.046(0.002)X	1.80(0.09)+0.048(0.002)X
$^{13}C^{16}O^b$	1.998(0.064)+0.1500(0.0028)X	1.680(0.021)+0.0124(0.0004)X
$^{12}C^{18}O^b$	1.70(0.06)+0.164(0.004)X	1.41(0.02)+0.0145(0.0002)X
$^{13}C^{18}O$	3.43(0.26)+0.173(0.021)X	3.41(0.34)

Notes. Previous values a: Eidelsberg (2012); b: Eidelsberg (2014).

Table 9. Comparison of SOLEIL predissociation rates for bands in the 4p5p region in various isotopologues (in units of 10^{11} s^{-1}), with $X = J'(J'+1)$.

Band upper level	Predissociation rates (10^{11} s^{-1})	
Isotopologue	*e*-parity	*f*-parity
4pπ $^1\Pi(2)$		
$^{12}C^{16}O^a$	0.80(0.03)+ 0.010(0.001)X	0.79(0.03)+ 0.009(0.001)X
$^{13}C^{16}O^b$	0.771(0.011)+0.0290(0.0047)X	0.763(0.008)+0.0160(0.0008)X
$^{12}C^{18}O^b$	0.910(0.045)+0.0294(0.0019)X	0.856(0.034)+0.0177(0.0008)X
$^{13}C^{18}O$	0.90(0.11)+0.041(0.005)X	1.00(0.11)+0.024(0.003)X
5pπ $^1\Pi(0)$		
$^{12}C^{16}O^a$	3.52(0.13)	3.52(0.13)
$^{13}C^{16}O^b$	$J' < 8$: 0.603(0.015)+0.0049(0.0002)X; $J' > 7$: 0.262(0.160)+0.0083(0.0011)X	0.550(0.028)+0.0056(0.0004)X
$^{12}C^{18}O^b$	$J' < 8$: 0.482(0.034)+0.0043(0.0013)X; $J' > 7$: 0.041(0.013)+0.0109(0.0011)X	0.471(0.028)+0.0038(0.0002)X
$^{13}C^{18}O$	0.54(0.11)+0.0011(0.0011)X	0.54(0.11)
5pσ $^1\Sigma^+(0)$		
$^{12}C^{16}O^a$	J' =0: 0.87(0.22); J' = 1–11: 2.4(0.4)+0.022(0.004)X; $J' > 11$: 2.4(0.4)	
$^{13}C^{16}O^b$	$J' < 6$: 0.147(0.017)+0.0402(0.0026)X; $J' > 5$: 2.05(0.09)+0.023(0012)X	
$^{12}C^{18}O^b$	$J' < 6$: 0.200(0.021)+0.0458(0.0013)X; $J' > 5$: 0.748(0.026)+0.026(0007)X	
$^{13}C^{18}O$	$J' < 8$: 0.226(0.024); $J' > 7$: –0.978(0.098)+0.018(0.003)X	

Notes. Previous values a: Eidelsberg (2012); b: Eidelsberg (2014).

the rare isotopologues of CO is not important due to their low column abundance. The consistency among results for the four isotopologues and the fact that the sum of oscillator strengths for the set of overlapping bands in the 92.5–93.5 nm region is isotopologue-independent give us confidence in our results.

Acknowledgements. We acknowledge SOLEIL for provision of synchrotron radiation facilities. All the data have been obtained on beamline DESIRS using the VUV-FTS spectrometer during proposals 20140051, 20120715, and 20110121. We acknowledge assistance from SOLEIL beamline staff (L. Nahon beamline scientist), NdO (VUV-FTS manager and co-author), and D. Joyeux (designer and builder of the VUV-FTS), for their constant help. This research was supported by funds from CNRS (France), Programme National Physico-Chimie du Milieu Interstellaire (PCMI), and NASA (grants NNG 06-GG70G and NNX10AD80G to the Univ. of Toledo and NNX09AC5GG to Wellesley College). J.R.L. and G.S. thank the NASA Origins of Solar System program (Grant NNX14AD49G) for funding. J.L.L. thanks the ISMO-CNRS (Institut des Sciences Moléculaires d'Orsay at Université Paris-Sud) for his welcome as honorary professor. This work is supported by the Dutch astrochemistry network (DAN) from the Netherlands Organisation for Scientific Research (NWO) under grant 648.000.002.

References

de Oliveira, N., Joyeux D., Phalippou, D., et al. 2009, Rev. Sci. Instr., 80, 043101
de Oliveira, N., Roudjane, M., Joyeux, D., et al. 2011, Nature Photonis, 5, 149
Eidelsberg, M., & Rostas, F. 1990, A&A, 235, 472
Eidelsberg, M., Roncin, J.-Y., Le Floch, A., et al. 1987, J. Mol. Spectr., 121, 309
Eidelsberg, M., Benayoun, J. J., Viala, Y. P., & Rostas, F. 1991, A&AS, 90, 231 (E91)
Eidelsberg, M., Lemaire, J. L., Fillion, J. H., et al. 2004, A&A, 424, 355
Eidelsberg, M., Sheffer, Y., Federman, S. R., et al. 2006, ApJ, 647, 1543 (E06)
Eidelsberg, M., Lemaire, J. L., Federman, S. R, et al. 2012, A&A, 543, 69 (E12)
Eidelsberg, M., Lemaire, J. L., Federman, S. R, et al. 2014, A&A, 2014, A&A, 566, 96 (E14)
Eikema, K. S. E., Hogervorst, W., & Ubachs, W. 1994, Chem. Phys., 181, 217
Federman, S. R., Fritts, M., Cheng, S., et al. 2001, ApJS, 134, 133
Gavilan, L., Lemaire, J. L., Eidelsberg, M., et al. 2013, J. Phys. Chem. A, 117, 9644
Heays, A. N., Dickenson, H., Salumbides, G. D., et al. 2011, J. Chem. Phys. 135, 4301
Heays, A. N., Eidelsberg, M., Lemaire, J. L., et al. 2014, J. Chem. Phys. 141, 144311
Herzberg, G. 1950, in Molecular spectra and molecular structure. Vol.1: Spectra of diatomic molecules, 2nd edn. (New York: Van Nostrand Reinhold), 280
Lefèbvre-Brion H. & Field R. W. 2004, The Spectra and Dynamics of Diatomic Molecules (Elsevier Academic Press)
Lefèbvre Brion, H., & Eidelsberg, M. 2012, J. Mol. Spectr., 271, 59
Lefèbvre-Brion H., & Majumder M. 2015, J. Chem. Phys., 142, 4306
Lefèbvre-Brion H., & Kalemos A. 2016, J. Chem. Phys., 144, 4302
Lemaire, J. L., Eidelsberg, M., Heays, A. N., et al. 2016, J. Phys. B, 49, 15, 4001
Morton, D. C., & Noreau, L. 1994, ApJS, 95, 301
Nahon, L., de Oliveira, N., Garcia, G., et al. 2013, J. Synchrotron. Rad., 19, 508
Rostas, F., Launay, F., Eidelsberg, M., et al. 1994, Can. J. Phys. 1994, 72, 913
Stark, G., Smith, P. L., Ito, K., & Yoshino, K. 1992, ApJ, 395, 705
Stark, G., Lewis, B. R., Gibson, S. T., & England, J. P. 1999, ApJ, 520, 732
Stark, G., Huber, K. P., Yoshino, K., Smith, P. L., & Ito, K. 2005, J. Chem. Phys., 123, 214303
Stark, G., Lewis, B. R., Heays, A. N., et al. 2008, J. Chem. Phys., 128, 114302
Stark, G., Heays, A. N., Lyons J. R., et al. 2014, ApJ. 788, 67
Tchang-Brillet, W.-Ü. L., Julienne, P. S., Robbe, J.-M., Letzelter, C., & Rostas, F. 1992, J. Chem. Phys., 96, 6735